Atmospheric Environment 219 (2019) 117051

Contents lists available at ScienceDirect

Atmospheric Environment

journal homepage: http://www.elsevier.com/locate/atmosenv

# Evaluating the methods and influencing factors of satellite-derived estimates of $NO_X$ emissions at regional scale: A case study for Yangtze River Delta, China

Yang Yang [a], Yu Zhao [a,b,*], Lei Zhang [a], Yi Lu [a]

[a] State Key Laboratory of Pollution Control, Resource Reuse and School of the Environment, Nanjing University, 163 Xianlin Ave., Nanjing, Jiangsu, 210023, China
[b] Jiangsu Collaborative Innovation Center of Atmospheric Environment and Equipment Technology (CICAEET), Nanjing University of Information Science, Technology, Jiangsu, 210044, China

## HIGHLIGHTS

- $NO_X$ emissions were constrained with the "synthetic" and real satellite observation.
- Influence of inversed approach on top-down estimates increased with finer resolution.
- Selection of satellite product was of great influence on NOx emission constraining.
- The model performance was largely improved with the optimized top-down estimates.

## ARTICLE INFO

*Keywords:*
$NO_X$ emissions
Top-down estimate
Satellite observation
YRD

## ABSTRACT

The top-down estimation of $NO_X$ emissions and their influencing factors were evaluated based on the "synthetic" and real satellite observation methods at different spatial scales in eastern China. Using the "synthetic" $NO_2$ vertical column densities (VCD) simulated from a hypothetical "true" emission inventory, the top-down estimates of $NO_X$ emissions for the Yangtze River Delta (YRD) region at 9 km resolution and the Southern Jiangsu City Cluster (SJC) at 3 km resolution were obtained using various inverse modeling approaches and the a priori emissions for January and July 2012. The normalized mean biases (NMBs) between the top-down and the hypothetical "true" emissions for all the cases were smaller than 6%, which indicates that both linear and nonlinear approaches could effectively constrain the total amount of emissions, with limited influence from spatial resolution, a priori emissions, and seasons. Larger differences for most cases were found for the normalized mean errors (NMEs), implying that the inverse modeling approach and other influencing factors played a more important role on the spatial distribution of the top-down estimates. Two $NO_2$ VCD products from real satellite observation (Dutch OMI $NO_2$ data product v2 (DOMINO v2) and Peking University OMI $NO_2$ data product v2 (POMINO v2)) were then applied to emissions constraints. The NMEs between the top-down estimates derived from the two products were calculated at 182% and 99% for January and July, respectively, indicating the great importance of satellite observation in constraining emissions. With the nonlinear inverse modeling approach, the top-down estimates of $NO_X$ emissions based on POMINO v2 were 25%–60% smaller than the national bottom-up inventory for the four seasons in the YRD, which indicates overestimation by the bottom-up method due to the insufficient consideration of recent air pollution control policy. At the 9 km resolution, the simulated $NO_2$ concentrations with air quality modeling based on the top-down estimates were much closer to available ground observation than the bottom-up ones for all seasons, which suggests improved emissions estimation from the inverse model at regional scales.

* Corresponding author. State Key Laboratory of Pollution Control, Resource Reuse and School of the Environment, Nanjing University, 163 Xianlin Ave., Nanjing, Jiangsu, 210023, China.
*E-mail address:* yuzhao@nju.edu.cn (Y. Zhao).

https://doi.org/10.1016/j.atmosenv.2019.117051
Received 11 June 2019; Received in revised form 23 September 2019; Accepted 10 October 2019
Available online 18 October 2019
1352-2310/

## 1. Introduction

Nitrogen oxides ($NO_X = NO_2 + NO$) are important precursors of secondary inorganic aerosols (SIA) and $O_3$. A $NO_X$ emission inventory is crucial to understand the atmospheric chemistry based on air quality modeling and is an important reference for formulating pollutant control measures. Emission inventories have been frequently developed using a bottom-up method, in which the emissions were calculated based on activity levels and emission factors by sector. For countries with large energy consumption and complicated source categories such as China, there are substantial biases in emission estimates with the bottom-up method, mainly attributed to the uncertainties of economy and energy statistics and those of emission factors due to insufficient field measurements (Granier et al., 2011; Ding et al., 2017; Zhao et al., 2017; Saikawa et al., 2017; Zhang et al., 2019). To improve the estimates, an inverse top-down method was developed to constrain the $NO_X$ emissions that combines the air quality model (AQM) and the satellite-derived troposphere vertical column density (VCD) of $NO_2$ (Kurokawa et al., 2009; de Foy et al., 2015; Zyrichidou et al., 2015; Kong et al., 2019). Among various instruments, including the Scanning Imaging Absorption Spectrometer for Atmospheric Chartography (SCIAMACHY), the Global Ozone Monitoring Experiment-2 (GOME-2) and the Ozone Monitoring Instrument (OMI), $NO_2$ VCDs from OMI were preferentially applied in constraining $NO_X$ emissions attributed to its higher

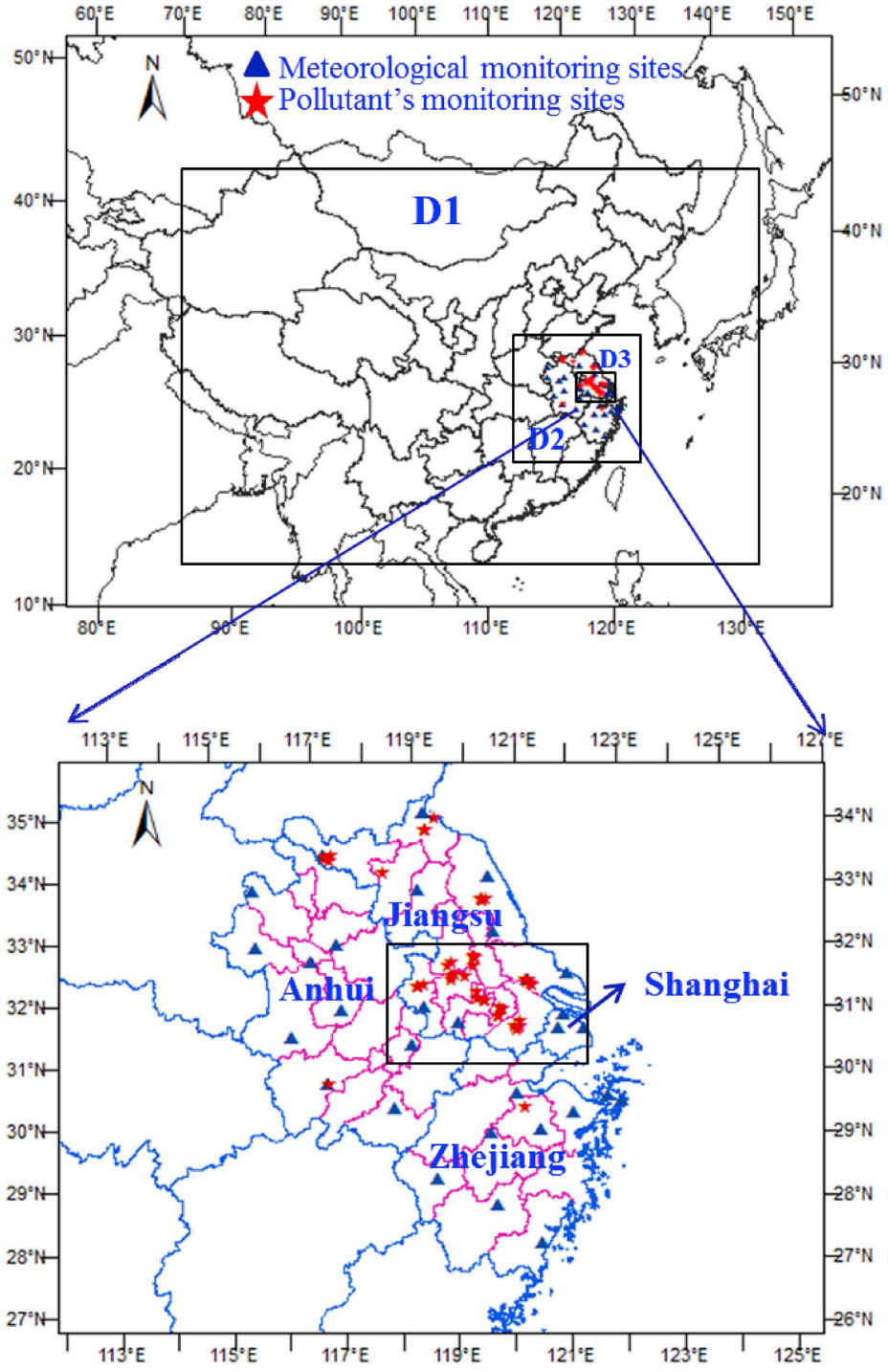


**Fig. 1.** Model domain and locations of meteorological and pollutant's monitoring sites.

temporal and spatial resolution (Jena et al., 2014; Zhao et al., 2018). Within mainland China, different OMI products were available including the Dutch OMI $NO_2$ data product v2 (DOMINO v2: Boersma et al., 2007; Boersma et al., 2011) and the Peking University OMI $NO_2$ data product v2 (POMINO v2: Lin et al., 2014; Lin et al., 2015; Liu et al., 2019).

There have been uncertainties in the top-down methods, and the top-down estimates of $NO_X$ emissions could be influenced by various factors including spatial resolution, a priori emissions, and satellite data (Lin et al., 2010; Cooper et al., 2017). For example, the difference of top-down $NO_X$ emissions in East Asia could reach 40% according to various studies (Ding et al., 2017). The error of top-down estimates increased by 82% when the spatial resolution was improved from 5° lat × 4° lon to lat 2.5° × lon 4° at the global scale (Cooper et al., 2017). The differences of top-down $NO_X$ emissions from various a priori emissions and satellite observation have been estimated at 14% in East Asia and 16–32% in China, respectively (Zhao and Wang, 2009; Gu et al., 2014). To better understand and improve the reliability of the top-down methodology, the inverse studies on $NO_X$ emissions should be carefully evaluated and the influencing factors should be identified. At present there are two types of methods for evaluation of the top-down estimation of $NO_X$ emissions. The first method was developed to examine the principle of the inverse top-down methodology (Cooper et al., 2017). The method assumed a bottom-up emission inventory as the hypothetical "true" inventory and the simulated $NO_2$ VCDs based on this inventory were determined as the "synthetic" satellite-derived $NO_2$ VCD. The $NO_X$ emissions were then estimated with the inverse top-down method and compared with the hypothetical true inventory. The second method applied the real satellite observation, and the top-down estimates of $NO_X$ emissions were assessed by comparing the simulated $NO_2$ concentrations with the AQM and those from ground observation (Liu et al., 2018a). In both methods, sensitivity analysis was commonly conducted to quantify the influences of various factors on the top-down estimates of $NO_X$ emissions (Gu et al., 2014; Cooper et al., 2017). Very few studies, however, have applied the two methods simultaneously, and a comprehensive understanding of the rationality and the factors that influence the top-down estimation of $NO_X$ emissions remains lacking, particularly for China with fast changes in energy use and emission control actions. In addition, current studies are usually conducted with relatively coarse horizontal spatial resolutions at the global (e.g., 2.5° lat × 4° lon) or the national scale (e.g., 70 × 70 $km^2$). In China, the policies of air pollution control are commonly implemented at the city level, and the inverse estimates and their evaluation with finer spatial resolution are thus greatly needed to improve the knowledge of emissions patterns and to detect the effectiveness of air pollution control at regional scales.

Located in eastern China, the Yangtze River Delta (YRD) region, including the city of Shanghai and the provinces of Anhui, Jiangsu and Zhejiang is one of the most developed regions and a hotspot of $NO_X$ emissions in the country (Li et al., 2017). With intensive industry and fossil fuel consumption, the southern Jiangsu cluster (SJC), which includes the cities of Suzhou, Wuxi, Changzhou, Zhenjiang and Nanjing is a typical region in the YRD greatly concerned with air quality improvement (Zhao et al., 2019). In this study, we chose the YRD and the SJC regions to evaluate the top-down estimates of $NO_X$ emissions and the factors that influence inverse modeling. Fig. 1 indicates the location and cities of the YRD region. Based on the "synthetic" satellite observation, we obtained and evaluated the top-down estimates for the YRD and the SJC at the resolutions of 9 and 3 km respectively, for January and July 2012. Different cases were set to explore the influence of inverse modeling, spatial resolution and a priori emissions on the top-down estimates. With the same options of season and spatial resolution, we then explored the factors that influence top-down estimates for YRD and SJC based on the real satellite observation. Model performance with the top-down estimates was further evaluated based on available ground observations. Finally, the top-down estimates of NOx emissions for January, April, July and October 2012 were developed with the optimized inverse modeling option, and the improvements against the bottom-up inventory were evaluated via the AQM and ground observations.

## 2. Data and methods

### 2.1. Evaluation of constrained emissions and influencing factors

Two methods, based on synthetic and real satellite observations (SSO and RSO respectively), were applied to evaluate the top-down estimates of $NO_X$ emissions and to identify the influencing factors. SSO applies the "synthetic" VCDs simulated from a hypothetical "true" inventory to constrain and correct the a priori emissions. Ideally, the top-down and the hypothetical "true" emissions should be very close to each other. The reliability and the robustness of the inverse modeling can then be evaluated by comparing' the hypothetical "true" and the derived top-down estimates. The difference between the two estimates could provide the uncertainty information of the method in an indirect way. Table 1 summarizes the settings of different cases using the SSO method. Two spatial scales, the YRD region with a 9 km resolution and the SJC region with a 3 km resolution were included in the analysis, and January and July were selected to represent different seasons. In addition, the nonlinear and linear approaches (described in Section 2.3) were separately applied to examine the influence of inverse modeling on emission estimates.

The Multi Resolution Emission Inventory for China 2012 (MEIC, http://www.meicmodel.org/) with an original spatial resolution of 0.1° × 0.1° was applied as the hypothetic "true" inventory for YRD region. A local inventory was compiled for Jiangsu by Zhou et al. (2017) with more detailed information on individual emission sources incorporated (JSEI, http://www.airqualitynju.com/), and was applied as the hypothetical "true" inventory for the SJC region. To evaluate the influence of the a priori emissions and spatial resolution, various inventories were applied in different cases: MEIC 2015 and MEIC 2012 were used as the a priori emissions for the YRD (Cases 1–4 in Table 1) and the SJC region (Cases 5–8 in Table 1), respectively. Moreover, in Cases 9–10 the a priori emissions were determined by doubling the total amount of the "true" inventory while keeping the emissions of each grid cell within the research domain at the same level (i.e., no spatial

**Table 1**
The information of cases based on synthetic satellite observation (SSO).

| | The a priori emissions | The "true" emissions | Method | Month | Resolution |
|---|---|---|---|---|---|
| Case1 | MEIC for 2015 | MEIC for 2012 | Linear | January | 9 km |
| Case2 | MEIC for 2015 | MEIC for 2012 | Nonlinear | January | 9 km |
| Case3 | MEIC for 2015 | MEIC for 2012 | Linear | July | 9 km |
| Case4 | MEIC for 2015 | MEIC for 2012 | Nonlinear | July | 9 km |
| Case5 | MEIC for 2012 | JSEI for 2012 | Linear | January | 3 km |
| Case6 | MEIC for 2012 | JSEI for 2012 | Nonlinear | January | 3 km |
| Case7 | MEIC for 2012 | JSEI for 2012 | Linear | July | 3 km |
| Case8 | MEIC for 2012 | JSEI for 2012 | Nonlinear | July | 3 km |
| Case9 | The modified "true" emissions | MEIC for 2012 | Nonlinear | January | 9 km |
| Case10 | The modified "true" emissions | JSEI for 2012 | Nonlinear | January | 3 km |

Note: The $NO_X$ emissions displayed in the table do not cover those from lighting and soil, and the emissions from the two sources are described in Section 2.4.

difference was assumed). The differences between the a priori and hypothetical "true" emission inventories are shown in Table S1 in the supplement. As seen in the table, the relative difference between the a priori and the "true" inventory was close for the YRD and the SJC for Cases 9–10, and the net influences of spatial resolution could thus be effectively evaluated.

To evaluate the error of top-down emissions estimation, the NMBs and NMEs between the top-down estimates and the hypothetical true emissions were used to evaluate the inverse approach, calculated with the following equations:

$$NMB = \frac{\sum_{i=1}^{n}(T_i - H_i)}{\sum_{i=1}^{n}(H_i)} \times 100\% \quad (1)$$

$$NME = \frac{\sum_{i=1}^{n}|T_i - H_i|}{\sum_{i=1}^{n}(H_i)} \times 100\% \quad (2)$$

where $T$ and $H$ indicate the top-down and hypothetical true $NO_X$ emissions, respectively, and $n$ indicates the number of model grids.

The setting of cases in the RSO method is summarized in Table 2. Similar to SSO, MEIC and JSEI were used as the a priori emissions for the YRD and the SJC, respectively, and the nonlinear and linear modeling were separately applied in January and July. The influence of satellite observations on top-down estimates was explored in RSO. Two products from OMI observations, POMINO v2 and DOMINO v2 (described in Section 2.2), were applied in the YRD region. Moreover, the averaging kernels (AKs) provide the relation between the retrieved $NO_2$ VCD and the hypothetical true $NO_2$ profile. To remove the errors from a priori $NO_2$ profile assumption in retrieved $NO_2$ VCD, AKs are recommended for application in the comparison between modeled and satellite-observed $NO_2$ VCD (Eskes and Boersma, 2003), and thus in the inverse constraints of $NO_X$ emissions (Han et al., 2015). Compared with other cases that applied AKs in the top-down estimation of $NO_X$ emissions, two cases using POMINO v2 were set using nonlinear modeling without AKs (Cases 4 and 8 in Table 2) to analyze the influence of AKs. The bottom-up and top-down estimates derived from nonlinear inverse modeling for the YRD and the SJC were evaluated with the AQM and ground-based observations of $NO_2$, and the improvement of top-down $NO_X$ emissions can be revealed.

### 2.2. Satellite observations

Tropospheric $NO_2$ VCDs were derived from the OMI onboard the Aura satellite, the local time of crossing the equator was 1:30 p.m. The spatial resolution for the OMI was 24 × 13 $km^2$ at the nadir (Levelt et al., 2006), one of the finest resolutions of $NO_2$ observation available before October 2017. Two products were applied for the YRD region in this work. The Dutch Ozone Monitoring Instrument $NO_2$ product (DOMINO v2) was developed by Boersma et al. (2011) and is available at http://www.temis.nl/airpollution/no2.html). Liu et al. (2019) developed an improved Peking University Ozone Monitoring Instrument $NO_2$ product (POMINO v2) for China upon DOMINO v2 that optimized the assumptions of the aerosol optical effect, surface reflectance anisotropy and vertical profiles of $NO_2$. The correlation coefficient ($R^2$) between POMINO v2 and available ground-based MAX-DOAS observations was 0.8, clearly higher than that of DOMINO v2 (0.64) (Liu et al., 2019). In POMINO v2 the $NO_2$ VCDs were used when the cloud fraction was less than 30%.

To match the resolution of AQM, the OMI $NO_2$ VCDs of Level-2 orbit product were resampled into an 18 km × 18 km grid system with the area weight method, and they were then downscaled to 9 km × 9 km and 3 km × 3 km with the Kriging interpolation method for the entire YRD and SJC regions, respectively. As an example, the $NO_2$ VCDs in July 2012 for the YRD and the SJC derived from POMINO v2 data are illustrated in the Fig. S1 in the supplement. The higher $NO_2$ VCDs were found in the east-central YRD and in the cities of Suzhou and Wuxi in the SJC.

**Table 2**
The information of cases based on real satellite observation (RSO).

| | The a priori emissions | Observation | Method | Month | Resolution |
|---|---|---|---|---|---|
| Case1 | MEIC for 2012 | POMINO v2 | Nonlinear | January | 9 km |
| Case2 | MEIC for 2012 | DOMINO v2 | Nonlinear | January | 9 km |
| Case3 | MEIC for 2012 | POMINO v2 without AKs | Nonlinear | January | 9 km |
| Case4 | MEIC for 2012 | POMINO v2 | Nonlinear | July | 9 km |
| Case5 | MEIC for 2012 | DOMINO v2 | Nonlinear | July | 9 km |
| Case6 | MEIC for 2012 | POMINO v2 without AKs | Nonlinear | July | 9 km |
| Case7 | JSEI for 2012 | POMINO v2 | Nonlinear | January | 3 km |
| Case8 | JSEI for 2012 | POMINO v2 | Nonlinear | July | 3 km |

Note: The $NO_X$ emissions displayed in the table do not cover those from lighting and soil, and the emissions from the two sources were described in Section 2.4.

### 2.3. Inverse modeling of $NO_X$ emissions

The linear (Jena et al., 2014; Gu et al., 2014) and nonlinear (Gu et al., 2016; Cooper et al., 2017) inverse modeling were applied in AQM to constrain NOx emissions. Linear inverse modeling assumes a constant linear correlation between the VCDs and emissions, and the top-down emissions were calculated with the following equations:

$$E_t = \alpha \times \Omega_o \quad (3)$$

$$\alpha = \frac{E_a}{\Omega_a} \quad (4)$$

where $E_t$ and $E_a$ represent the top-down and a priori emissions, $\Omega_o$ and $\Omega_a$ represent the observed $NO_2$ and modeled VCD, and $\alpha$ represents the linear coefficient between VCD and emissions.

The nonlinear inverse modeling assumed variable nonlinear correlation between $NO_2$ VCDs and emissions, and the top-down emissions were calculated with the following equations:

$$E_t = E_a\left(1 + \frac{\Omega_o - \Omega_a}{\Omega_o}\beta\right) \quad (5)$$

$$\frac{\triangle E}{E} = \beta\frac{\triangle \Omega}{\Omega} \quad (6)$$

where $\beta$ represents the response coefficient of the simulated $NO_2$ VCD to a certain change in emissions. The changed fraction of a priori emissions was set at 10% in this work, and its influence on the top-down $NO_X$ emissions was small based on testing. $\beta$ was calculated with the changed fraction of the a priori emissions and the corresponding changed modeled VCD. The constrained daily emissions with the top-down method were treated as the a priori emission of the next day, and constraining would continue until the change of NME between the top-down and the a priori emission was below 1% for e successive times.

### 2.4. Model configuration

The Models-3 Community Multi-scale Air Quality (CMAQ) version 4.7.1 was applied to constrain and evaluate the $NO_X$ emissions. As illustrated in Fig. 1, three nested domains were applied in the Lambert Conformal Conic projection centred at (110°E, 34°N), with spatial resolutions of 27, 9 and 3 km, respectively. The mother domain (D1, 177 × 127 cells) covered most parts of China, North and South Korea, and a few parts of Japan, whereas the second (D2, 118 × 121 cells) and third domains (D3, 133 × 73 cells) covered the entire YRD and SJC regions, respectively. The spin-up period in this study was 5 days. The

boundary condition of D1 was taken from clean air, and those of D2 and D3 were taken from the modeled results of D1 and D2, respectively. The height of the first model layer was approximately 60 m, and the PBL scheme of the model was ACM2 (Pleim, 2007). Details on model configuration were described in Zhou et al. (2017) and Yang and Zhao (2019).

As described in Section 2.1, the emissions of anthropogenic origin in D1 and D2 were obtained from MEIC, and those in D3 were taken from Zhou et al. (2017). The original horizontal resolution of MEIC was 0.1° × 0.1°. The emissions of residential sources were downscaled to 9 km according to the spatial distribution of population, and the emissions of power, industry and transportation were downscaled to 9 km according to that the spatial distribution of gross domestic product (GDP). Biogenic emissions was from the Model Emissions of Gases and Aerosols from Nature developed under the Monitoring Atmospheric Composition and Climate project (MEGAN MACC, Sindelarova et al., 2014), and the emissions of Cl, HCl and lightning $NO_X$ were from the Global Emissions Initiative (GEIA, Price et al., 1997). The $NO_X$ emissions from soil were collected from Yienger and Levy (1995), and were doubled as suggested by Zhao and Wang (2009) and Lin et al. (2010). Biomass open burning was not included in the CMAQ simulation, because the open biomass burning of ~70% for YRD was concentration in June (Yang and Zhao, 2019) and it has a little influence on the results of other months.

Meteorological fields were provided by the Weather Research and Forecasting Model (WRF) version 3.4, and the domain and vertical setting was consistent with the CMAQ. The outputs were transferred by the meteorology chemistry interface professor (MCIP) version 4.2 into the chemistry transport module in CMAQ. The simulated parameters from WRF for D2 and D3 in January, April, July and October 2012 were compared with the observation dataset of the US National Climate Data Center (NCDC), as summarized in Table S2 and S3 in the Supplement. For D2, the average biases of wind speed for the four months between the two datasets were smaller than 0.2 m/s. The root mean square deviation (RMSE) of wind direction for the four months between the two datasets were close to or smaller than 45°, and the indexes of agreement (IOAs) of temperature and relative humidity between the two datasets were higher than 0.7. The meteorological parameters for D2 and D3 were in compliance with the benchmarks derived from Emery et al. (2001) and Jiménez et al. (2006).

The hourly $NO_2$ concentrations of 43 stations in 12 cities and daily $NO_2$ concentrations of 2 cities were used to evaluate the $NO_X$ emission inventories. The hourly $NO_2$ concentrations were derived from the China National Environmental Monitoring Center (http://www.cnemc.cn/). The daily $NO_2$ concentrations for the cities of Anqing and Shaoxing were obtained from the local environmental protection bureau (http://aqxxgk.anqing.gov.cn//list.php?unit=HA028,xxflid=32060100 and http://sxepb.sx.gov.cn/col/col1488046/index.html). Locations of the ground observation stations are indicated in Fig. 1.

## 3. Results and discussion

### 3.1. Evaluation based on synthetic satellite observation (SSO)

Shown in Fig. 2 are the differences between the top-down $NO_X$ estimates and the hypothetical true $NO_X$ emission inventory in Cases 1–8 using the SSO method. In general, the NMBs for all the cases were smaller than 6%, which implies that the total amount of $NO_X$ emissions could be well constrained based on the nonlinear and linear inverse modeling. Moreover, the results indicated that the influences on the total amount of the constrained top-down $NO_X$ emissions were limited by the changes in inverse modeling (linear or nonlinear), spatial resolution, the a priori emissions and season. Larger differences of NMEs were found for most cases, which implies that the spatial distribution of the top-down estimate depended more on the inverse modeling and relevant influencing factors. Fig. S2 in the supplement shows the spatial distribution of $NO_X$ emissions in MEIC for D2 at the horizontal resolution of 9 km and that in JSEI for D3 at the resolution of 3 km in July 2012. By comparing Fig. 2 with Fig. S2, larger differences between the top-down and the "true" estimates were detected in the area with relatively high emissions, e.g., the east-central YRD region and the urban area of Nanjing in the SJC.

The NMEs between the hypothetical true and the top-down estimates based on the nonlinear inverse modeling were smaller than those based on the linear modeling in all the cases in Fig. 2, and the maximum was calculated at 25.9% for the SJC region at a resolution of 3 km for January (Fig. 2f). The largest and smallest difference of NMEs between the nonlinear/linear inverse modeling result and the "true" emissions were found for the SJC region (3 km resolution) in January (9.5%, panels e and f) and for the YRD region (9 km resolution) in July at (1.9%, panels c and d), respectively. The results suggest that the $NO_X$ emissions could be effectively constrained with the nonlinear inverse approach compared to the linear one and that the nonlinear method should preferentially be selected for the top-down estimation of $NO_X$ emissions. Principally the relationship between $NO_X$ emissions and $NO_2$ VCDs could be better captured with a nonlinear constraint approach (Gu et al., 2016). The relationships between $NO_X$ emissions and $NO_2$ VCDs should be nonlinear. It was mainly because that the photochemical feedbacks between NOx and OH were nonlinear (Gu et al., 2016). In low $NO_X$ emission condition, the increase of $NO_X$ emission promotes the OH production and reduces its lifetime, and increase of $NO_X$ emission restrains the OH production and increases its lifetime in high $NO_X$ emission condition. Fig. S3 in the supplement shows the variation of NME between the top-down and hypothetical true $NO_X$ estimates for the YRD region during the iteration processes with the linear and nonlinear inverse modeling. The average difference of NME between the linear and nonlinear inverse modeling in the iterations was 0.8% in July, clearly smaller than that in January (4.1%). As the relationship between $NO_X$ emissions and $NO_2$ VCD was closer to linear when the $NO_2$ VCD was smaller (Gu et al., 2016), the influence of the inverse modeling approach was small in summer.

With the same inverse modeling approach, a priori emissions and spatial resolution, the top-down estimates in July were closer to the hypothetical true emissions than those in January, indicated by the smaller NMEs. Similarly, Cooper et al. (2017) found that the NMEs between the hypothetical true emissions at the global scale and the top-down estimate derived with nonlinear modeling approach at a spatial resolution of 2° lat × 2.5° lon was larger in January than in July. The possible reason was that the regional transport of $NO_X$ becomes easier with longer distances due to a longer lifetime in winter and some emissions were thus harder to be constrained in the correct area. In summer, the faster dispersion of $NO_X$ can be expected in the YRD region, attributed to higher temperature and stronger oxidation, thus the top-down methodology could be more applicable. The largest difference in NME between January and July was found at 13.7% in the cases with the linear modeling approach at 3 km resolution (panels e and g). The results indicate that the influence of seasonal meteorology on $NO_X$ emissions constraint would be enhanced with linear inverse modeling, particularly at finer resolution.

Cases 9–10 explored the influences of spatial resolution and the a priori emissions on the top-down estimation of $NO_X$ emissions; the differences between the top-down and hypothetical true emissions are shown in Fig. 3. Similar to Fig. 2, the NMB for all the cases in Fig. 3 were smaller than 3%. The results again suggest that nonlinear inverse modeling was effective in the calculation of the total amount of $NO_X$ emissions. With fixed season and spatial resolution, the NMEs for all cases in Fig. 3 were larger than those in Fig. 2. The maximum growth of NME was 6.7% in winter at 3 km resolution (Fig. 3b versus Fig. 2f). The result implies that the influence of the a priori emissions on the inverse modeling should be considered, and that the improvement in detailed information of emissions sources in the bottom-up inventory was helpful

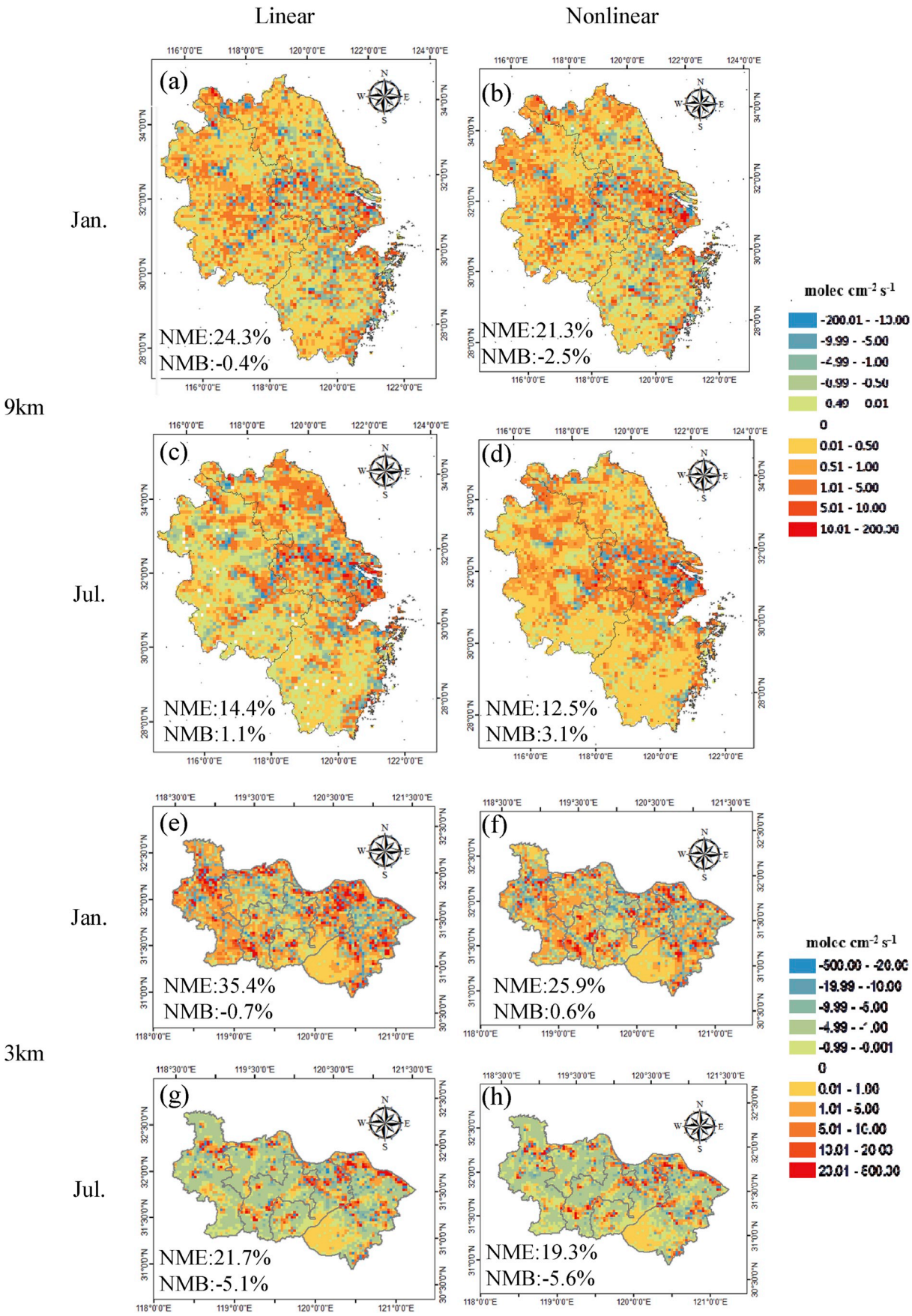


**Fig. 2.** The differences between the top-down estimates and hypothetical true $NO_X$ emissions based on Cases 1–8 in Table 1.

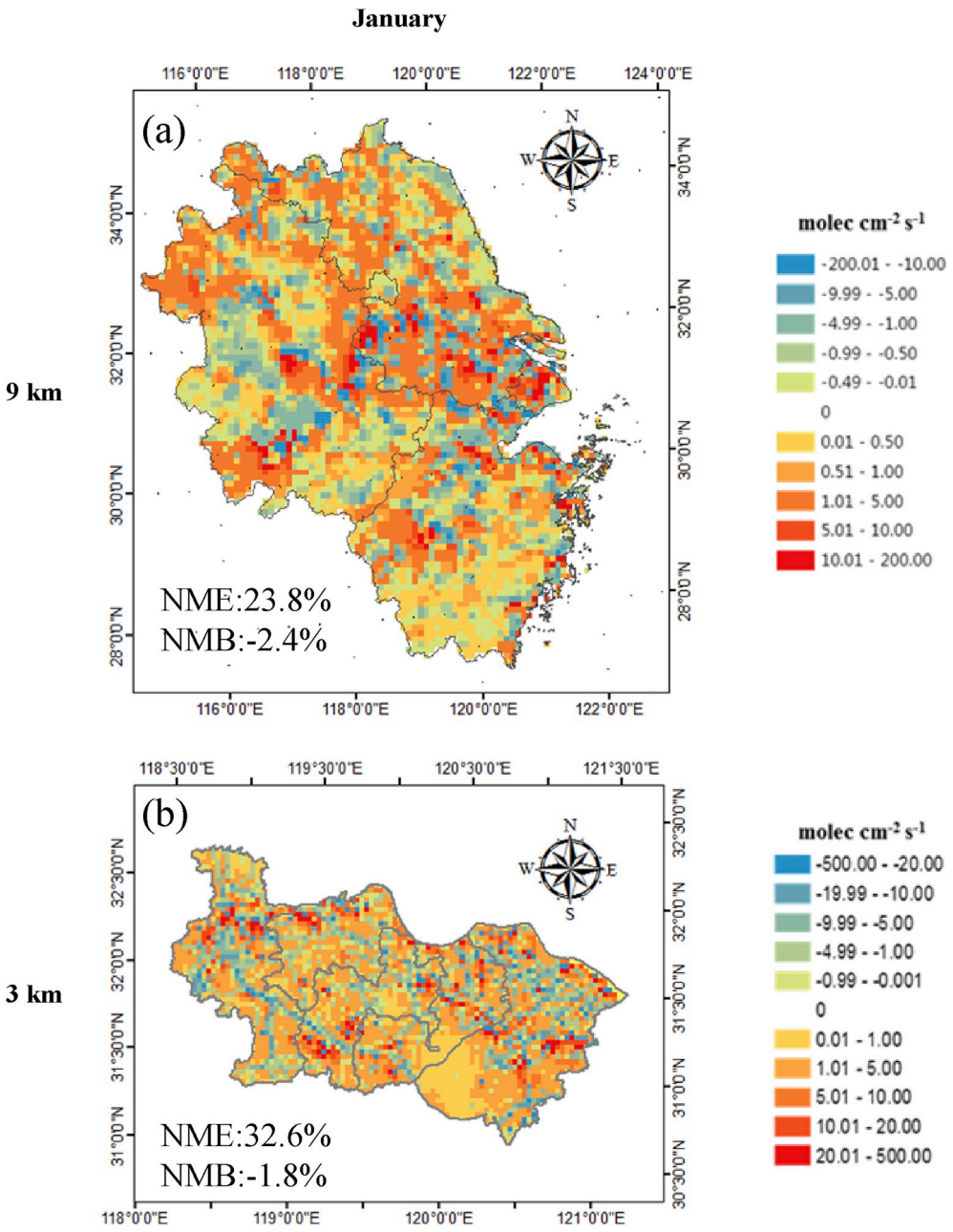


**Fig. 3.** The differences between the top-down estimates and hypothetical true $NO_X$ emission inventories based on Cases 9–10 in Table 1.

for the evaluation of the emissions from a top-down perspective as well, particularly at finer spatial resolution. Remarkably, the average NME between the a priori and the hypothetical true emissions for Cases 9–10 was 2.6 times larger than that for Cases 2 and 4; however, the analogue number declined to 0.2 times between the top-down and the hypothetical true emissions. The result suggests that the top-down modeling approach would reduce the bias between the a priori and the hypothetical true emissions via the inverse constraint of emissions.

With other influencing factors fixed, the NMEs with 9 km resolution (Fig. 3a) were smaller than those with 3 km resolution (Fig. 3b), which indicates that the top-down estimates with coarser resolution could be more reliable. A similar result was found by Cooper et al. (2017) that the NMEs between the "true" emissions and the top-down estimates declined when 4° lat × 5° lon resolution instead of 2° lat × 2.5° lon was applied in the nonlinear inverse modeling for January. With finer AQM resolution, more emissions could be expected to transport into neighboring grids and thus lead to bias in the top-down estimation. The accuracy of the a priori emission could also be a challenge for AQM at finer resolution, as more detailed information of emission sources should be collected (Zheng et al., 2017).

### 3.2. Evaluation based on real satellite observation (RSO)

Based on the nonlinear modeling approach, the $NO_X$ emissions were constrained with POMINO v2 and DOMINO v2 for the YRD region at the resolution of 9 km, and the differences (DOMINO v2 minus POMINO v2) between the top-down estimates with the two satellite products are shown in Fig. 4. The NMEs for January and July were calculated at 182.0% and 99.1%, respectively. The corresponding NMEs of $NO_2$ VCDs between DOMINO v2 and POMINO v2 were estimated to be 48.9% and 25.8% for January and July, respectively, as shown in Fig. S4 in the supplement. The result indicates that the influence of satellite data is considerable in both winter and summer, and that the selection of appropriate satellite data is crucial to constrain $NO_X$ emissions. Both the

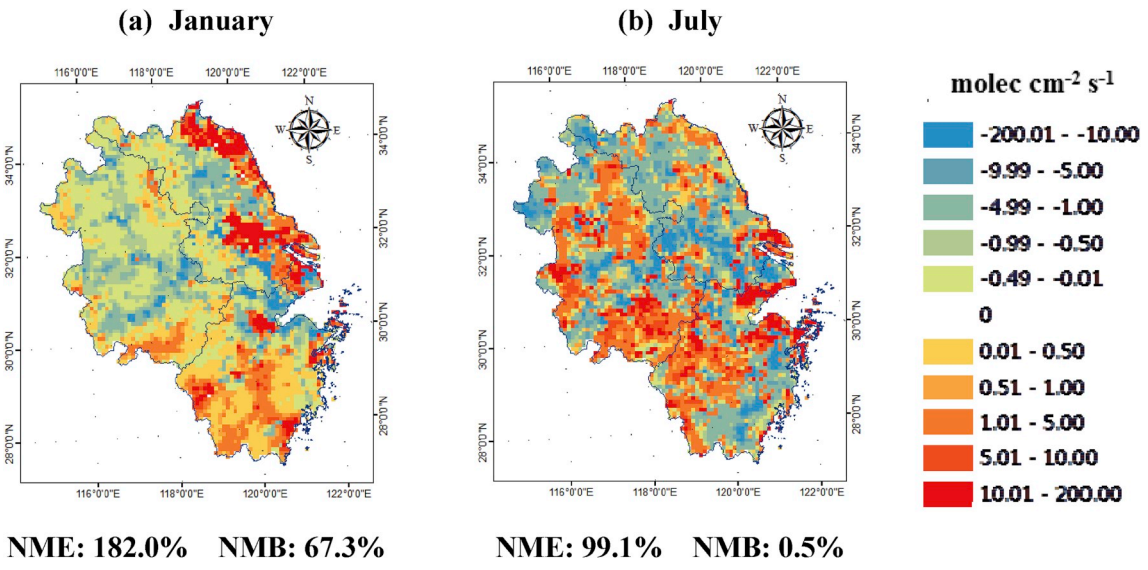


**Fig. 4.** The differences (DOMINO v2 minus POMINO v2) between the top-down $NO_X$ estimates based on DOMINO v2 and POMINO v2 for YRD with the nonlinear approach (panel a derived from Cases 1 and 2 in Table 2; panel b derived from Cases 4 and 5 in Table 2; The NMB and NME were calculated with the equations (S1) and (S2) in the supplement).

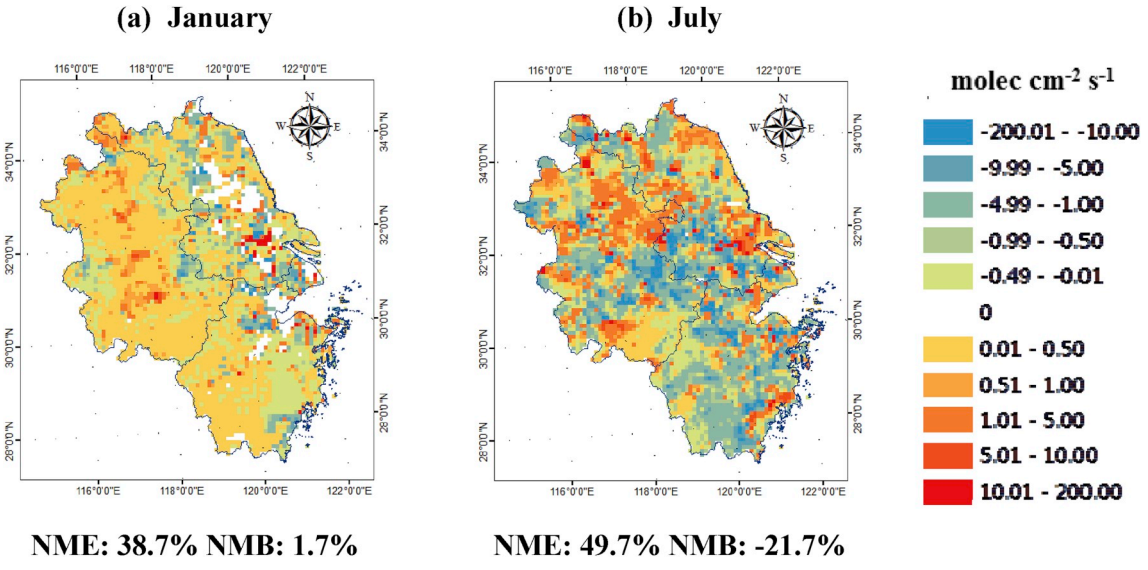


**Fig. 5.** The differences (without AKs minus with AKs) between top-down $NO_X$ estimates derived without and with AKs based on nonlinear approach and POMINOv2 data (panel a derived from Cases 2 and 3 in Table 2; panel b derived from Cases 5 and 6 in Table 2; The NMB and NME were calculated with the equations (S3) and (S4) in the supplement).

NMBs and NMEs in January were clearly larger than those in July, which implies that satellite data played a more important role on $NO_X$ emissions constraining in winter. Since POMINO v2 made important progress in the aerosol optical effect on retrieval of satellite data, its influence on $NO_X$ constraint is expected to be greater in winter due to the higher aerosol concentration than in summer. The NMB between the constrained $NO_X$ emissions with DOMINO v2 and POMINO v2 was only 0.5% in July, which implies that the influence of satellite data on the total $NO_X$ emissions was small in summer. Regarding the spatial deviation, the constrained emissions from DOMINO v2 were larger than those from POMINO v2 in eastern and southern of Jiangsu and smaller in the east-central YRD in January, which mainly resulted from the difference in spatial distribution of $NO_2$ VCD from DOMINO v2 and POMINO v2, as shown in Fig. S4.

Fig. 5 shows the difference (without AKs minus AKs) between the top-down estimates without and with AKs based on the nonlinear modeling approach and POMINO v2 for the YRD region. The NMEs between the constrained emissions for January and July were calculated at 38.7% and 49.7%, respectively, implying that the influence of AKs on $NO_X$ constraint should be taken seriously in both winter and summer. Substantial uncertainty exists in the top-down $NO_X$ emission estimation without AKs. The NMB and NME in July were larger than those in January, implying that the influence of AKs on top-down $NO_X$ emissions in summer could be greater than in winter. A similar result was found for Europe that the influence of AKs on the comparison of simulated and observed $NO_2$ VCD in summer was larger than in winter (Boersma et al., 2016). The larger differences were commonly found in the east-central YRD with intensive $NO_X$ emissions, which implies the enhanced importance of AKs on emission constraining for those areas. Because the influence of the a priori $NO_2$ profile assumption on retrieving of $NO_2$ was expected to be larger in the regions with higher emissions (Boersma et al., 2016), application of AKs in those regions could more effectively

**Table 3**
Model performance statistics for $NO_2$ concentrations between observation and CMAQ simulation with the a priori and top-down $NO_X$ estimates in January and July 2012.

$$NMB = \frac{\sum_{i=1}^{n}(M_i - O_i)}{\sum_{i=1}^{n}(O_i)} \times 100\%, \quad NME = \frac{\sum_{i=1}^{n}|M_i - O_i|}{(O_i)} \times 100\%$$

| | | | January | | July | |
|---|---|---|---|---|---|---|
| | | | The a priori | Top-down | The a priori | Top-down |
| **9 km** | Hourly | NMB | 56.4% | 34.8% | 109.6% | 43.7% |
| | | NME | 57.0% | 39.7% | 110.6% | 49.4% |
| | Daily | NMB | 56.4% | 34.8% | 109.8% | 43.6% |
| | | NME | 56.4% | 36.2% | 109.8% | 43.6% |
| **3 km** | Hourly | NMB | 49.2% | 49.7% | 44.9% | 55.4% |
| | | NME | 53.0% | 53.8% | 57.1% | 64.0% |
| | Daily | NMB | 49.1% | 49.6% | 44.8% | 55.3% |
| | | NME | 49.3% | 49.6% | 45.2% | 55.3% |

Note: NMB and NME were calculated using the following equations (*M* and *O* indicate the results from modeling prediction and observation, respectively).

reduce the bias from the a priori $NO_2$ profile.

### 3.3. Evaluation with the AQM and ground observations

CMAQ simulation was conducted for both the a priori and the top-down estimates of $NO_X$ emissions derived from the nonlinear approach for the YRD (Cases 2 and 6 in Table 2) and those for the SJC (Cases 10 and 12 in Table 2). The model performances are summarized in Table 3 for January and July 2012, indicated by the comparisons between the simulated and observed ground $NO_2$ concentrations. The NMB and NME derived from the a priori emissions in the SJC were smaller than those in YRD. It was mainly because that the bottom-up emission inventory for SJC (JSEI) was developed at the city level and incorporated most available information about industrial plants and vehicles, and the uncertainty of the inventory was expected to be reduced compared with the national inventory (MEIC) for the smaller SJC region (Zhou et al., 2017).

The NMBs and NMEs based on the top-down estimates were smaller than those based on the a priori emissions for both January and July in the YRD at the resolution of 9 km. The better modeling performance from ground observation indicates that the $NO_X$ emission estimation could be improved via the top-down constraint with satellite observations at the regional scale. In contrast, at the city-cluster scale with 3 km resolution, the NMBs and NMEs based on the top-down estimates were equal to or larger than those based on the a priori emission for both January and July. The result implies that the $NO_X$ emission estimates at very fine spatial resolution could hardly be improved by the inverse modeling with current products of satellite-derived $NO_2$ VCDs probably because there was uncertainty in the inverse approach and satellite observations at finer resolution. Given that the estimates of $NO_X$ emissions at both 9 km and 3 km resolution could be improved in SSO method described in Section 3.1, the relatively poor top-down estimates with high temporal resolution from the RSO method at city cluster scale resulted largely from the coarse spatial resolution of OMI. However, the emissions with high spatial resolution might be developed by sacrificing the temporal resolution (Kong et al., 2019).

### 3.4. Comparison and evaluation of the bottom-up and satellite-derived top-down estimates of emissions in the YRD

According to the evaluation with the AQM and ground observations, the best option of inversing $NO_X$ emissions for YRD region was identified as application of POMINO v2 with the nonlinear inverse modeling at the resolution of 9 km. With this optimized option, the top-down estimates of YRD $NO_X$ emissions were derived for January, April, July and October 2012, and the monthly total emissions of the bottom-up (MEIC, 2012) and the top-down estimates are shown in Fig. 6. The top-down estimates were smaller than the a priori emissions for the four months, which implies that current bottom-up inventory might overestimate the emission for all seasons. On average, the monthly emissions from the top-down estimation were calculated at 219 Gg/month, 44% smaller than those from the a priori emissions. The largest and smallest overestimations were found in January and April, and the top-down estimates were 60.4% and 24.6% smaller than the a priori emissions, respectively. Similar result was found by Qu et al. (2017), who suggested that China's $NO_X$ emissions for 2012 were overestimated by 45% in the bottom-up inventory. Consistent with the results for the entire country in Qu et al. (2017), both the bottom-up and top-down estimates of this work found the largest and smallest $NO_X$ emissions in summer and winter, respectively, However, the ratio of summer to winter emissions in the top-down estimation was 2.07, much larger than that of 1.17 in the bottom-up inventory. The results indicate that the seasonal variation of $NO_X$ emissions could potentially be underestimated in the bottom-up inventory.

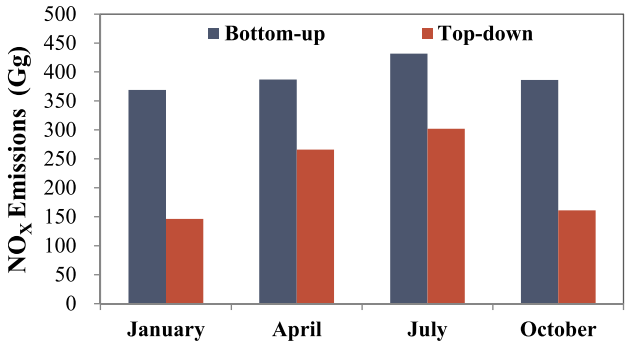


**Fig. 6.** The total bottom-up and top-down $NO_X$ emissions derived from the nonlinear method and POMINOv2 data for YRD in January, April, July and October 2012.

The spatial differences of the bottom-up and top-down estimates of $NO_X$ emissions in January, April, July and October 2012 are shown in Fig. 7, and the bottom-up and top-down emissions of YRD in January, April, July and October of 2012 are shown in Fig. S5 in the supplement. The top-down estimates were smaller than the bottom-up $NO_X$ emission inventories in the east-central YRD with high emissions, which implies that overestimation in the bottom-up inventory commonly exists in the region with higher emissions. In contrast, the top-down estimates were larger than the bottom-up estimates in most of Zhejiang with relatively small emissions. On one hand, the emissions in the region were probably allocated in the developed areas due to use of the distribution coefficient of the GDP or population. On the other hand, some emission sources in this region could be missed in the country level emission inventory due to the difficulty of collecting information. The overestimation for the developed areas largely resulted from the insufficient consideration of improved emission controls in the current bottom-up inventory (Zhou et al., 2017; Zhang et al., 2019). To improve air quality, the government has been conducting a series of emission control measures, particularly on big power and industrial sources with relatively large emissions. Consequently, the emissions from those sources could be considerably reduced, mainly due to the improved removal efficiency of pollutant control devices. However, such information could hardly be full captured in bottom-up inventories, particularly at the national scale. Moreover, increasing numbers of plants have been moved from developed regions to suburban or less-developed regions, although, the economic indicators (such as gross domestic product) and population were still applied to allocate the emissions if the precise locations of those

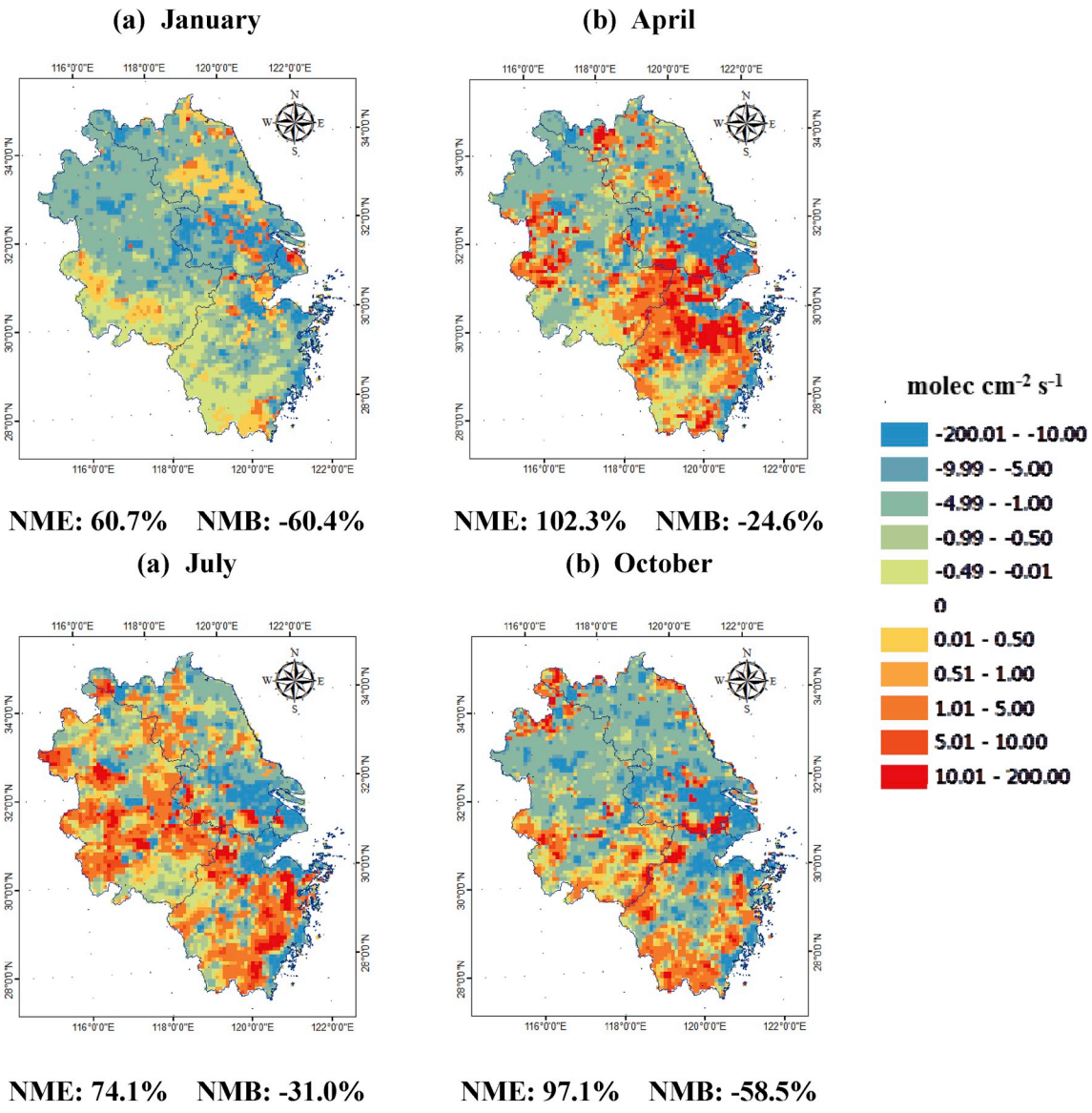


**Fig. 7.** The spatial differences (top-down minus bottom-up) between the top-down $NO_X$ emission inventories and bottom-up $NO_X$ estimates derived from the nonlinear method and POMINOv2 data for YRD in January, April, July and October 2012 (The NMB and NME were calculated with the equations (S5) and (S6) in the supplement).

plants were unclear or not timely recorded, which led to elevated emissions in the developed regions such as the east-central YRD.

The observed and simulated hourly $NO_2$ concentrations using the bottom-up and top-down estimates are shown in Fig. 8 for January, April, July and October 2012 (note that the NMEs and NMBs for January (panel a) and July (panel c) are provided in Table 3 as well). The observational data were taken from the 43 stations of China National Environmental Monitoring Center, as shown in Fig. 1. For all the simulated months, the simulated $NO_2$ concentrations derived with bottom-up $NO_X$ inventories were clearly larger than the observations in the two months, which again indicates the overestimation of the bottom-up estimates on $NO_X$ emissions. Much better model performance was achieved with the top-down estimates compared with that with the bottom-up ones, which largely resulted from the improvement in $NO_X$ emissions estimation with the inverse constraining approach based on satellite observations. Larger NMB and NME were found in summer. On one hand, the sensitivity of $NO_2$ concentration to emissions was larger in summer than in winter (Gu et al., 2016), and stronger changes in simulated concentrations were thus expected in summer, with similar changes in emissions. On the other hand, the error could be relevant for the simulation of meteorological parameters such as wind speed. In the WRF modeling, the wind speed was underestimated by 8% for July and the average error for the other months was only 4%.The largest improvement on the model performance based on the top-down estimate instead of the bottom-up one was found for July, and the NMBs and NMEs were respectively reduced by 65.9% and 61.2%. Because the $NO_2$ concentration was expected to respond more strongly to the change in emissions in summer, more effective improvement of modeling performance was expected with the constrained top-down estimate of $NO_X$ emissions in the season. Remarkably, there were some problems in PBL schemes of CMAQ before version 5.1 that led to overestimation of diurnal variation of $NO_2$ and differences between simulations and observations (Liu et al., 2018b).

The uncertainties of top-down estimation of $NO_X$ emissions for the YRD were mainly associated with the inverse modeling approach, satellite observations and the AQM. The NMBs and NMEs between the top-down estimates based on the nonlinear inverse approach and the hypothetical "true" emissions in the SSO method were −5.6%–3.1% and 12.5%–32.6%, respectively. The results suggested that uncertainty existed in the inverse approach. The uncertainty of observed $NO_2$ VCDs

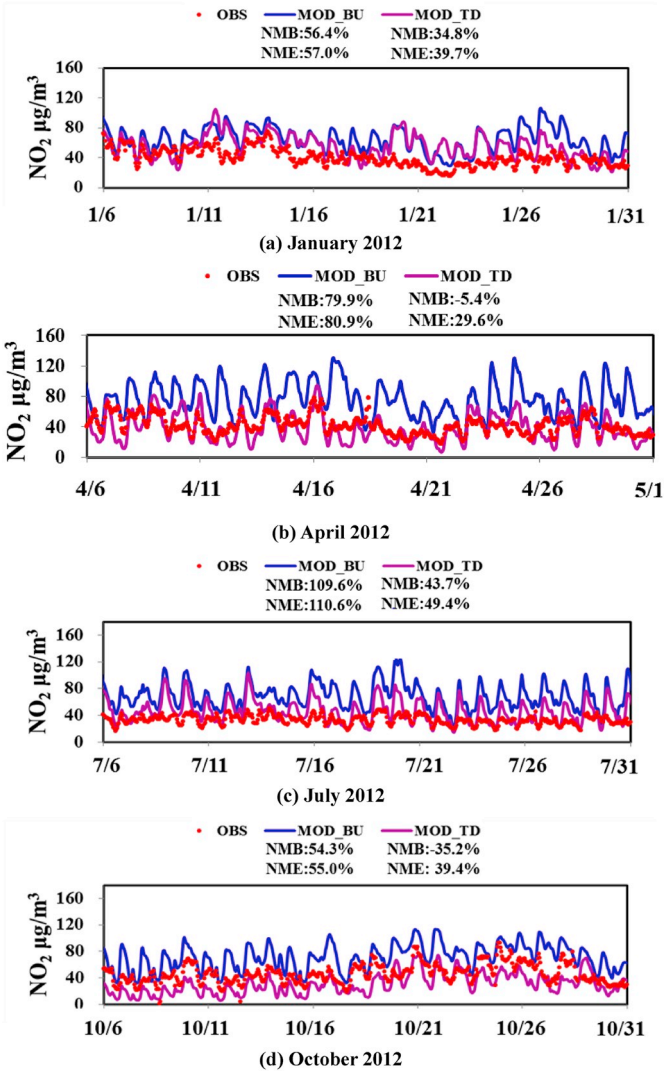


**Fig. 8.** Observed and simulated hourly $NO_2$ concentrations based on bottom-up (MOD_BU) and top-down (MOD_TD) $NO_X$ emissions in January, April, April and October 2012.

could reach 29.4% in cloud-free days (Liu et al., 2019), which implies that the bias from satellite observation was an important source of the uncertainty in the top-down estimation of $NO_X$ emissions. The AQM uncertainty was associated with meteorological fields and chemistry mechanisms and its overall uncertainty is difficult to be quantified at present. Specially, the problems in PBL schemes of CMAQ before version 5.1 also brought some uncertainties (Liu et al., 2018b). Better top-down estimates could be expected with improvement in AQM in the future.

## 4. Conclusions

Taking the YRD and the SJC region in China as examples, we comprehensively evaluated the top-down estimates of $NO_X$ emissions and relevant influencing factors based on synthetic and real satellite observations. The total amounts of emissions could be well constrained and were slightly influenced by the inverse approach, the a priori emissions, and the horizontal resolution, while the seasonal and spatial distribution of emissions largely depended on them. Substantial difference between the top-down estimates derived from DOMINO v2 and POMINO v2 implied that the appropriate satellite data were of great importance in constraining $NO_X$ emissions. The estimation of $NO_X$ emissions could be improved based on the nonlinear inverse modeling approach at the resolution of 9 km, whereas the bias was elevated at 3 km resolution probably due to the coarser spatial resolution of OMI. Overestimation in $NO_X$ emissions was indicated in the current bottom-up inventory for the YRD region, and the model performance with the top-down estimates was largely improved for all seasons compared with that with the bottom-up estimates, particularly for summer. Better top-down estimates at the regional scale could be expected along with optimized new satellite observation products at finer resolution (e.g., TROPOMI) in the future.

## Declaration of competing interest

The authors declare that they have no known competing financial interests or personal relationships that could have appeared to influence the work reported in this paper.

## Acknowledgements

This work was sponsored by Natural Science Foundation of China (91644220 and 41922052) and the National Key Research and Development Program of China (2017YFC0210106). We would also like to thank Tsinghua University for the free use of national emissions data (MEIC), and TEMIS and Peking University for the support of satellite data (POMINO v2 and DOMINO v2, respectively).

## Appendix A. Supplementary data

Supplementary data related to this article can be found at https://doi.org/10.1016/j.atmosenv.2019.117051.

## References

Boersma, K.F., Eskes, H.J., Veefkind, J.P., Brinksma, E.J., van der, A.R.J., Sneep, M., van den Oord, G.H.J., Levelt, P.F., Stammes, P., Gleason, J.F., Bucsela, E.J., 2007. Near-real time retrieval of tropospheric $NO_2$ from OMI. Atmos. Chem. Phys. 7, 2103–2118.

Boersma, K.F., Eskes, H.J., Dirksen, R.J., van der A, R.J., Veefkind, J.P., Stammes, P., Huijnen, V., Kleipool, Q.L., Sneep, M., Claas, J., Leitao, J., Richter, A., Zhou, Y., Brunner, D., 2011. An improved retrieval of tropospheric $NO_2$ columns from the ozone monitoring instrument. Atmos. Meas. Tech. 4, 1905–1928.

Boersma, K.F., Vinken, G.C.M., Eskes, H.J., 2016. Representativeness errors in comparing chemistry transport and chemistry climate models with satellite UV–Vis tropospheric column retrievals. Geosci. Model Dev. (GMD) 9, 875–898.

Cooper, M., Martin, R.V., Padmanabhan, A., Henze, D.K., 2017. Comparing mass balance and adjoint methods for inverse modeling of nitrogen dioxide columns for global nitrogen oxide emissions. J. Geophys. Res.: Atmosphere 122, 4718–4734.

de Foy, B., Lu, Z., Streets, D.G., Lamsal, L.N., Duncan, B.N., 2015. Estimates of power plant NOx emissions and lifetimes from OMI $NO_2$ satellite retrievals. Atmos. Environ. 116, 1–11.

Ding, J.Y., Miyazaki, K., van der, R.J., Mijling, B., Kurokawa, J., Cho, S.Y., Greet Janssens-Maenhout, G., Zhang, Q., Liu, F., Levelt, P.F., 2017. Intercomparison of NOx emission inventories over East Asia. Atmos. Chem. Phys. 17, 10125–10141.

Emery, C., Tai, E., Yarwood, G., 2001. Enhanced Meteorological Modeling and Performance Evaluation for Two Texas Episodes, Report to the Texas Natural Resources Conservation Commission. International Corp, Novato, CA prepared by ENVIRON.

Eskes, H.J., Boersma, K.F., 2003. Averaging kernels for DOAS total column satellite retrievals. Atmos. Chem. Phys. 3, 1285–1291.

Granier, C., Bessagnet, B., Bond, T., Angiola, A.D., van der, G.H.D., Frost, G.J., Heil, A., Kaiser, J.W., Kinne, S., Klimont, Z., Kloster, S., Lamarque, J.F., Liousse, C., Masui, T., Meleux, F., Mieville, A., Ohara, T., Raut, J.C., Riahi, K., Schultz, M.G., Smith, S.J., Thompson, A., van Aardenne, J., van der Werf, G.R., van Vuuren, D.P., 2011. Evolution of anthropogenic and biomass burning emissions of air pollutants at global and regional scales during the 1980–2010 period. Clim. Change 109, 163–190.

Gu, D.S., Wang, Y.X., Smeltzer, C., Boersma, K.F., 2014. Anthropogenic emissions of NOx over China: Reconciling the difference of inverse modeling results using GOME-2 and OMI measurements. J. Geophys. Res.: Atmosphere 119, 7732–7740.

Gu, D.S., Wang, Y.H., Yin, R., Zhang, Y.Z., Smeltzer, C., 2016. Inverse modelling of NOx emissions over eastern China: uncertainties due to chemical non-linearity. Atmos. Meas. Tech. 9, 5193–5201.

Han, K.M., Lee, S., Chang, L.S., Song, C.H., 2015. A comparison study between CMAQ-simulated and OMI-retrieved $NO_2$ columns over East Asia for evaluation of NOx emission fluxes of INTEX-B, CAPSS, and REAS inventories. Atmos. Chem. Phys. 15, 1913–1938.

Jena, C., Ghude, S.D., Beig, G., Chate, D.M., Kumar, R., Pfister, G.G., Lal, D.M., Surendran, D.E., Fadnavis, S., van der A, R.J., 2014. Inter-comparison of different

$NO_X$ emission inventories and associated variation in simulated surface ozone in Indian region. Atmos. Environ. 17, 61–73.
Jiménez, P., Jorba, O., Parra, R., Baldasano, J.M., 2006. Evaluation of MM5-EMICAT2000-CMAQ performance and sensitivity in complex terrain: high-resolution application to the northeastern Iberian Peninsula. Atmos. Environ. 40, 5056–5072.
Kong, H., Lin, J.T., Zhang, R.X., Liu, M.Y., Weng, H.J., Ni, R.J., Chen, L.L., Wang, J.X., Zhang, Q., 2019. High-resolution ($0.05^\circ \times 0.05^\circ$) NOx emissions in the Yangtze River Delta inferred from OMI. Atmos. Chem. Phys. 19, 12835–12856.
Kurokawa, J.I., Yumimoto, K., Uno, I., Ohara, T., 2009. Adjoint inverse modeling of NOx emissions over eastern China using satellite observations of $NO_2$ vertical column densities. Atmos. Environ. 43, 1878–1887.
Levelt, P.F., Hilsenrath, E., Leppelmeier, G.W., van den Oord, G.H.J., Bhartia, P.K., Tamminen, J., de Haan, J.F., Veefkind, J.P., 2006. Science objectives of the ozone monitoring instrument. IEEE Trans. Geosci. Remote Sens. 44, 1199–1208.
Li, M., Zhang, Q., Kurokawa, J.i., Woo, J.H., He, K., Lu, Z., Ohara, T., Song, Y., Streets, D. G., Carmichael, G.R., Cheng, Y., Hong, C., Huo, H., Jiang, X., Kang, S., Liu, F., Su, H., Zheng, B., 2017. MIX: a mosaic Asian anthropogenic emission inventory under the international collaboration framework of the MICS-Asia and HTAP. Atmos. Chem. Phys. 17, 935–963.
Lin, J.T., McElroy, M.B., Boersma, K.F., 2010. Constraint of anthropogenic $NO_X$ emissions in China from different sectors: a new methodology using multiple satellite retrievals. Atmos. Chem. Phys. 10, 63–78.
Lin, J.T., Martin, R.V., Boersma, K.F., Sneep, M., Stammes, P., Spurr, R., Wang, P., Van Roozendael, M., Clémer, K., Irie, H., 2014. Retrieving tropospheric nitrogen dioxide from the Ozone Monitoring Instrument: effects of aerosols, surface reflectance anisotropy, and vertical profile of nitrogen dioxide. Atmos. Chem. Phys. 14, 1441–1461.
Lin, J.T., Liu, M.Y., Xin, J.Y., Boersma, K.F., Spurr, R., Martin, R., Zhang, Q., 2015. Influence of aerosols and surface reflectance on satellite $NO_2$ retrieval: seasonal and spatial characteristics and implications for NOx emission constraints. Atmos. Chem. Phys. 15, 11217–11241.
Liu, F., van der, A.R., Eskes, H., Ding, J., Mijling, B., 2018. Evaluation of modeling $NO_2$ concentrations driven by satellite-derived and bottom-up emission inventories using in situ measurements over China. Atmos. Chem. Phys. 18, 4171–4186.
Liu, M.Y., Lin, J.T., Wang, Y.C., Sun, Y., Zheng, B., Shao, J., Chen, L.-L., Zheng, Y., Chen, J., Fu, M., Yan, Y.-Y., Zhang, Q., Wu, Z., 2018. Spatiotemporal variability of $NO_2$ and $PM_{2.5}$ over Eastern China: observational and model analyses with a novel statistical method. Atmos. Chem. Phys. 18, 12933–12952.
Liu, M.Y., Lin, J.T., Boersma, K.F., Pinardi, G., Wang, Y., Chimot, J., Wagner, T., Xie, P., Eskes, H., Van Roozendael, M., Hendrick, F., Wang, P., Wang, T., Yan, Y.Y., Chen, L. L., Ni, R.J., 2019. Improved aerosol correction for OMI tropospheric NO2 retrieval over East Asia: constraint from CALIOP aerosol vertical profile. Atmos. Meas. Tech. 12, 1–21.
Pleim, J.E., 2007. A combined local and nonlocal closure model for the atmospheric boundary layer. part I: model description and testing. J. Appl. Meteorol. Climatol. 46, 1383–1395.
Price, C., Penner, J., Prather, M., 1997. $NO_X$ from lightning, Part I: global distribution based on lightning physics. J. Geophys. Res. Atmos. 102, D5.
Qu, Z., Henze, D.K., Capps, S.L., Wang, Y., Xu, X., Wang, J., Keller, M., 2017. Monthly top-down NOx emissions for China (2005–2012): a hybrid inversion method and trend analysis. J. Geophys. Res. Atmos. 122, 4600–4625.
Saikawa, E., Kim, H., Zhong, M., Zhao, Y., Janssens-Maenhout, G., Kurokawa, J., Klimont, Z., Wagner, F., Naik, V., Horowitz, L.W., Zhang, Q., 2017. Comparison of emissions inventories of anthropogenic air pollutants and greenhouse gases in China. Atmos. Chem. Phys. 17, 6393–6421.
Sindelarova, K., Granier, C., Bouarar, I., Guenther, A., Tilmes, S., Stavrakou, T., Müller, J. F., Kuhn, U., Stefani, P., Knorr, W., 2014. Global data set of biogenic VOC emissions calculated by the MEGAN model over the last 30 years. Atmos. Chem. Phys. 14, 9317–9341.
Yang, Y., Zhao, Y., 2019. Quantification and evaluation of atmospheric pollutant emissions from open biomass burning with multiple methods: a case study for Yangtze River Delta region, China. Atmos. Chem. Phys. 19, 327–348.
Yienger, J.J., Levy II, H., 1995. Empirical model of global soil biogenic $NO_X$ emissions. J. Geophys. Res. 100, 11447–11464.
Zhang, Y., Bo, X., Zhao, Y., Nielsen, C.P., 2019. Benefits of current and future policies on emission reduction from China's coal-fired power sector indicated by continuous emission monitoring. Environ. Pollut. 251, 415–424.
Zhao, C., Wang, Y., 2009. Assimilated inversion of $NO_X$ emissions over east Asia using omi $NO_2$ column measurements. Geophys. Res. Lett. 36 (6), 1–6.
Zhao, Y., Zhou, Y.D., Qiu, L.P., Zhang, J., 2017. Quantifying the uncertainties of China's emission inventory for industrial sources: from national to provincial and city scales. Atmos. Environ. 165, 207–221.
Zhao, Y., Xia, Y., Zhou, Y., 2018. Assessment of a high-resolution $NO_X$ emission inventory using satellite observations: a case study of southern Jiangsu, China. Atmos. Environ. 190, 135–145.
Zhao, X.F., Zhao, Y., Chen, D., Li, C.Y., Zhang, J., 2019. Top-down estimate of black carbon emissions for city clusters using ground observations: a case study in southern Jiangsu, China. Atmos. Chem. Phys. 19, 2095–2113.
Zheng, B., Zhang, Q., Tong, D., Chen, C.C., Hong, C.P., Li, M., Geng, G.N., Lei, Y., Huo, H., He, K.B., 2017. Resolution dependence of uncertainties in gridded emission inventories: a case study in Hebei, China. Atmos. Chem. Phys. 17, 921–933.
Zhou, Y.D., Zhao, Y.D., Mao, P., Zhang, Q., Zhang, J., Qiu, L.P., Yang, Y., 2017. Development of a high-resolution emission inventory and its evaluation and application through air quality modeling for Jiangsu Province, China. Atmos. Chem. Phys. 17, 211–233.
Zyrichidou, I., Koukouli, M.E., Balis, D., Markakis, K., Poupkou, A., Katragkou, E., Kioutsioukis, I., Melas, D., Boersma, K.F., van Roozendael, M., 2015. Identification of surface $NO_X$ emission sources on a regional scale using OMI $NO_2$. Atmos. Environ. 101, 82–93.